Probing Molecular Binding Effect from Zinc Oxide Nanocrystal Doping in Surface-Stabilized Ferroelectric Liquid Crystal with Two-Dimensional Infrared Correlation Technique

Jung Y. Huang,* Liu S. Li, and Ming C. Chen

Department of Photonics and Institute of Electro-Optical Engineering, Chaio Tung University, Hsinchu, Taiwan

Received: November 11, 2007; In Final Form: January 26, 2008

Doping liquid crystal (LC) with nanomaterials has been shown to yield some degrees of freedom for tailoring LC properties. This approach can be employed to produce new LC materials with high application potentials by blending instead of synthesizing new mesogenic molecules. In this paper, we show that doping ferroelectric liquid crystal (FLC) with ZnO nanocrystals improves the alignment order of a surface-stabilized FLC (SSFLC) in both steady-state and field-induced reorientation processes. We used the two-dimensional infrared (2D IR) correlation technique to reveal that the ZnO nanocrystals were uniformly dispersed into the FLC medium. The homogeneous dispersion of ZnO nanodots produces stronger correlations among the IR-active molecular normal modes of FLC molecules, which then leads to more concerted reorientation process at the submolecular level. A molecular binding effect originating from a dipolar interaction of the ZnO nanodot with surrounding C═O groups of FLC molecules was proposed to illustrate our measured results. We estimated the total energy reduced by the doping to be about 1000 J/m^3. The alignment stability gained is similar to that experienced by FLC molecules within 100-nm distance to an alignment surface with a strong anchoring strength of 1×10^{-4} J·m^{-2}.

Introduction

Ferroelectric liquid crystals (FLCs) can be used for flat panel displays (FPD) with advantages of fast response, bistability, and wide viewing angle.[1,2] However, the availability of FLC FPD is quite limited at present. One major reason is a mechanical problem with destruction of the smectic layer structure by a mechanical shock, which could render the device useless. Furthermore, industrial applications of FLC FPD often require FLC materials to meet some stringent criteria of optical, viscoelastic properties, and a wide temperature range of the SmC* mesophase. Recent studies have revealed that doping LC with nanomaterials can provide some degree of freedom for tailoring material properties.[3−5] Therefore, FLC materials with high application potential can be prepared by blending instead of synthesizing new mesogenic molecules.

Currently the mechanical problems of FLC FPD are still quite challenging to deal with. Although the stability of the layer structure of FLC can be improved by embedding the smectic layer structure in a photopolymer matrix,[6] the improvement was achieved by sacrificing the fast response of FLC molecules. To devise an effective scheme for layer stabilization without sacrificing the fast response of FLC, insight into intermolecular interaction is indispensable. To probe into the intermolecular interaction and the resulting structural changes of FLC molecules during the field-induced reorientation,[7−12] time-resolved Fourier transform infrared (FTIR) absorption spectroscopy had been widely employed. It was noted that upon the reversal of the sign of an applied electric field on a FLC film all of the molecules switch by rotation about a tilted SmC* cone. This is because coupling with the applied electric field is through ferroelectric polarization, not through coupling with any individual molecular dipoles. An issue remaining is whether FLC molecules in SmC* reorient like a deformable molecule or like a rigid body.[13] Two-dimensional infrared correlation (2D IR) spectroscopy can be an ideal choice to clarify this issue.[14]

Two-dimensional infrared correlation is a technique where the spectral intensity is plotted as a function of two independent spectral variables. By spreading spectral peaks along the second dimension, one can gain the advantage of sorting out complex or overlapped spectral features that normally cannot be resolved in a one-dimensional spectrum.[15−19] Generalized 2D IR spectroscopy is an effective mathematical tool to elucidate the spectral details of a dynamic system. The data yielded from the technique are usually presented with *synchronous* and *asynchronous* plots.[20] The synchronous plot reveals the information about the in-plane order and the similarity in the IR azimuthal angular patterns, whereas the asynchronous plot offers the information about the dissimilarity in the azimuthal angular patterns.[21]

In this paper, we applied the 2D IR correlation technique to show that ZnO nanocrystals (*nc*-ZnO) can be dispersed uniformly into an FLC host and the uniform doping leads to an improved alignment structure of FLC. We proposed that the ZnO nanodots tie up surrounding FLC dipolar species and yield a molecular binding effect.

Experimental Section

Materials. Zinc oxide nanocrystals (*nc*-ZnO) were prepared in view of the low-cost synthetic process with nontoxic chemicals. To obtain a stabilized *nc*-ZnO colloid, we coated the *nc*-ZnO with 3-(trimethoxysilyl) propyl methacrylate (TPM)

* Corresponding author. E-mail: jyhuang@faculty.nctu.edu.tw; 886-3-5716631 (Fax); 886-3-5731975 (Tel).

10.1021/jp710778s CCC: $40.75
Published on Web 03/18/2008

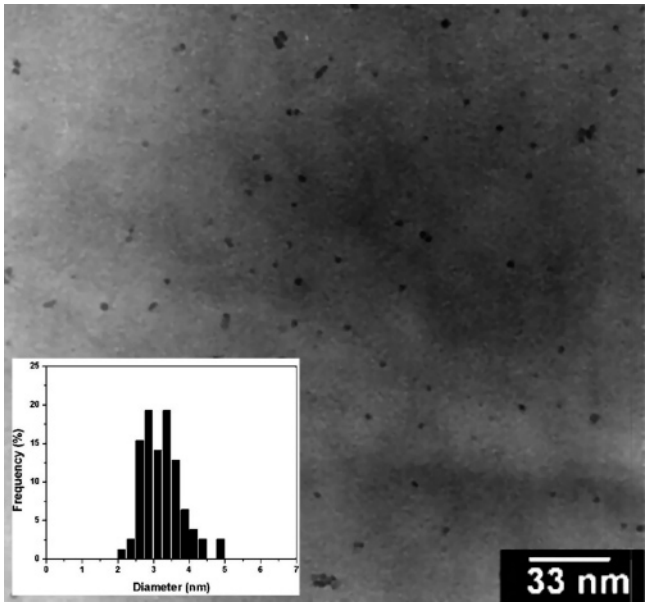

Figure 1. TEM image and size distribution histogram (inset) of fresh unmodified ZnO particles.

and purified the colloid by following to the reported procedure.[22,23] The TEM image shown in Figure 1 reveals the *nc*-ZnO colloid to have a size distribution of a mean diameter of 3.2 nm and a full width at half-maximum (fwhm) of 1 nm.

The SSFLC test cells comprise two CaF_2 plates coated with indium tin oxide (ITO) and RN1182 polyimide (from Nissan Chemical) alignment layers rubbed unidirectionally along the *Z* axis, as shown in Figure 2. Two substrates with antiparallel rubbing were assembled into a test cell with a gap of 1.5 μm, approximating to the half-wave thickness $d_{\lambda/2} = \lambda/2\Delta n = 1.9$ μm estimated with $\Delta n = 0.17$ and $\lambda = 0.633$ μm. We used Felix 17/100 (from Hoechst, Germany) as the FLC host in view of its excellent device application properties. The FLC material exhibits a thermotropic transition sequence of $Cr \xleftrightarrow{-28°C} SmC^* \xleftrightarrow{73°C} SmA^* \xleftrightarrow{77°C} N^* \xleftrightarrow{85°C} Iso$.[24]

To prepare *nc*-ZnO doped SSFLC, we dispersed an appropriate amount of *nc*-ZnO nanopowder into Felix 017/100 with ultrasonic at 85 °C for 40 min. The resulting medium with 1.0 wt % *nc*-ZnO was filled into test cells and then cooled slowly to 35 °C to form a stable single SmC* domain. Because the ZnO nanocrystals have a dimension compatible to the smectic C* layer spacing, the layer structure cannot be changed significantly by doping; therefore, *nc*-ZnO shall behave like a molecular dopant.

***CV* Characterization of the SSFLC Test Cells.** The *C*−*V* measurements of the SSFLC test cells were carried out with a computer-controlled HP4284A LCR meter, which provides a bias voltage range of ±35 V with a sinusoidal wave of 1.0 V in a frequency range of 20 Hz−1 MHz. The spontaneous polarization vector of a SSFLC cell can be aligned parallel to the direction of an applied electric field on the cell. The switching of the spontaneous polarization vector can be accompanied by a change of the applied electric field. This yields a nonlinear contribution to the capacitance C_{LC} of the SSFLC cell[25]

$$C_{LC} = C_{lin} + \left(\frac{dP}{dV_{ext}}\right)\frac{A}{L} \qquad (1)$$

where V_{ext} denotes the applied voltage and *A* and *L* are the area and the thickness of the FLC capacitor, respectively.

The nonlinear part of the FLC capacitance can be deduced with the Preisach model, assuming that the individual FLC dipoles add up to form the total polarization *P* and each of them exhibits a rectangular hysteretic loop. For the case of FLC with multiple dipolar species, the cell capacitance can be expressed as[26]

$$C_{LC} = C_{lin} + \sum_i \frac{(FP_s)_i\,\delta_i}{\cosh^2\left[\delta_i(V_{ext} \mp V_{Ci}^{\pm})\right]}\frac{A}{L} \qquad (2)$$

Here $(FP_s)_i$ indicates the portion of the *i*th dipolar species in the non-saturated switching loop; $V_{Ci}^{\pm}$ denotes the mean value of the individual coercive voltage; and $\delta_i = \log\{[1 + (P_r/P_s)_i]/[1 - (P_r/P_s)_i]\}/V_{Ci}$ is a species-related constant with P_r and P_s being the remnant and saturation polarizations. The (±) sign refers to an increasing/decreasing V_{ext}. Equation 2 shows that the capacitance peak in the *C*−*V* curve results from the polarization reversal with a peak height relating to the amount of switchable polarization.[27]

FTIR Measurement and 2D IR Correlation Analysis. Figure 2 presents the schematic of a SSFLC cell in an infrared absorption spectrometer. Time-resolved FTIR spectra from 900 to 3500 cm^{-1} with 4-cm^{-1} resolution were recorded with a liquid-nitrogen-cooled HgCdTe detector and a homemade data acquisition electronics.[21,28] Bipolar square-wave pulses were used to drive the test cell. The waveform is comprised of a +10 V pulse extending from 0 to 140 μs, followed by a field-free period from 140 to 500 μs. Then a −10 V pulse extends from 500 to 640 μs, followed by a field-free duration from 640 to 1000 μs. For each polarization direction of the incident infrared beam, a total of 32 time-resolved interferograms were acquired. The 2D correlation analysis with varying infrared polarization angles were calculated based upon an algorithm developed by Noda,[29] and was implemented in a software 2Dshige by S. Morita.[30]

Experimental Results

We presented in Figure 3 the measured CV characteristic curves (filled symbols: negative-to-positive sweep; open symbols: positive-to-negative sweep) of a undoped (3a) and a *nc*-ZnO doped SSFLC (3b) at a frequency of 1 kHz. For a satisfactory fit to eq 2, the undoped SSFLC cell requires three dipolar species, shown in Figure 3a with the dashed, short-dashed, and dash−dotted curves. The result is reasonable in viewing that the FLC material FELIX 017-100 is in fact a mixture comprising several FLC dipolar species, which respond differently to different field strengths and frequencies. For the *nc*-ZnO doped SSFLC, only a single species is needed for a satisfactory fit, indicating that doping with *nc*-ZnO simplifies the response to an applied electric field significantly.

By inserting the SSFLC cell into a crossed polarizer−analyzer setup and rotating the cell about the beam propagation direction, an azimuthal optical transmittance pattern with four-folded symmetry can be observed.[26] The results were presented in Figure 3c. The transmited optical intensity can be described by

$$I_T(t) = I_o \sin^2\left(\frac{\Gamma}{2}\right)\cos^2[2\theta + 2\phi(t)] \qquad (3)$$

where $\Gamma = 2\pi\langle\Delta n\rangle/\lambda = [2\pi\Delta n_0/\lambda]\cdot S$ with *S* denoting the order parameter. Very small light leakage in the dark states indicates that the SSFLC test cells possess fairly good quality of molecular alignment. The bright state of the *nc*-ZnO doped cell was found to have 2.3-times higher optical transmittance than that of the

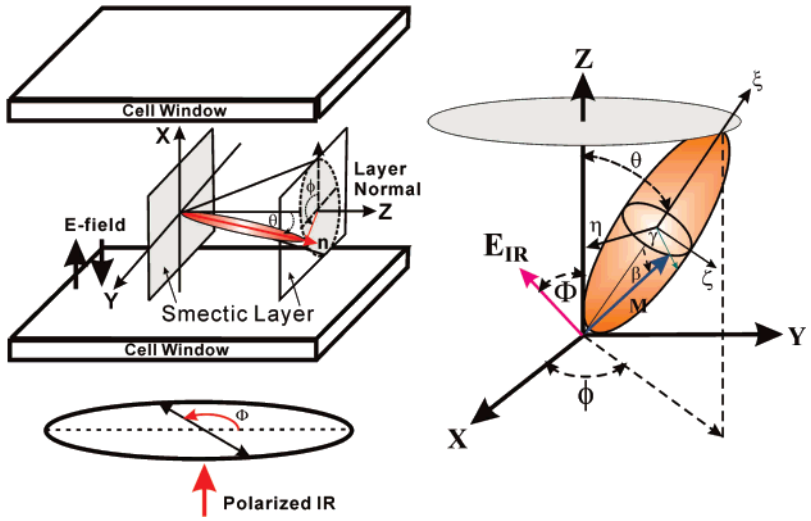

Figure 2. Schematic of SSFLC cell for the time-resolved infrared absorption measurements. *Z* denotes the rubbing direction, which is also the layer normal of the smectic layers. **E** is the direction of the applied electric field. M on the right diagram denotes the IR dipole, which tilts from the molecular long axis ξ with an angle β and can rotate about the ξ axis by γ.

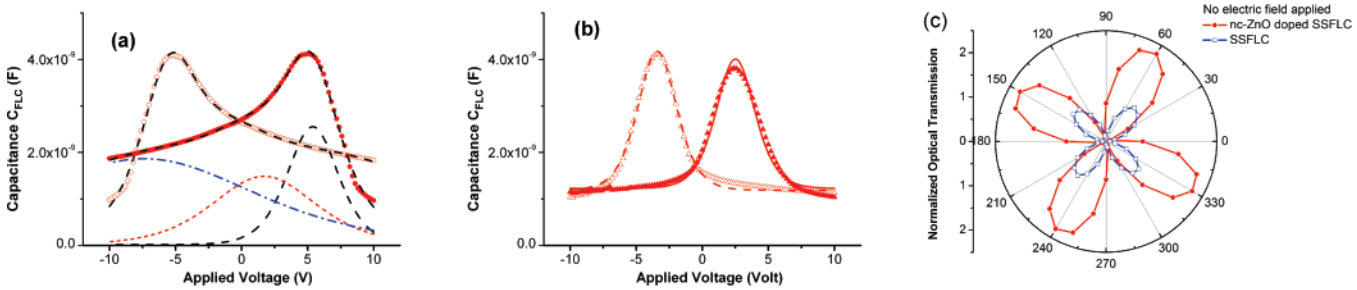

Figure 3. Experimental $C-V$ characteristics (symbols) at 1 kHz and their fitting curves of the SSFLC cells (a) without and (b) with *nc*-ZnO doping. In Figure 3a, the three curves with dash, short-dash, and dash−dot, respectively, represent the three Preisach terms involved in the negative-to-positive sweep CV curve. (c) The normalized field-free azimuthal optical transmittance patterns of the pure SSFLC (open squares) and the nc-ZnO doped SSFLC (filled circles) were presented.

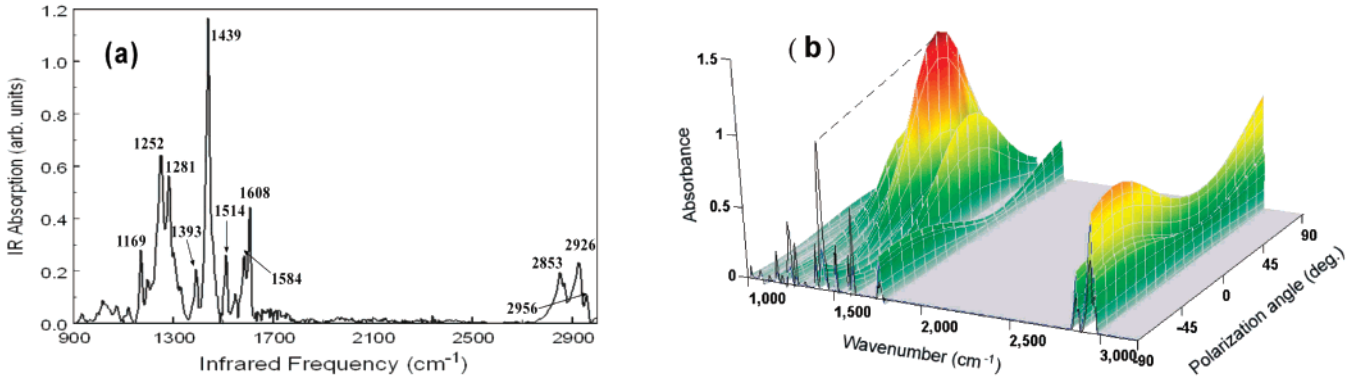

Figure 4. (a) Infrared absorption spectrum of FELIX 017/100 SSFLC at 35 °C and $\Phi = 0°$. (b) A set of polarized IR spectra for a *nc*-ZnO-doped FELIX 017/100 SSFLC cell at 35 °C and without an applied electric field for IR polarization angle Φ in the range $-90° \rightarrow +90°$. The incident IR polarization angle is taken as zero when its polarization direction coincides with the rubbing direction (i.e., the Z axis).

undoped cell. The increased optical transmittance with *nc*-ZnO doping can be attributed to higher *S* and lower scattering loss.

We applied FTIR to probe into the alignment at the submolecular level. An IR beam with varying polarization direction was normally incident on a SSFLC cell. Depending upon the orientation, each functional group will experience a different IR field component. A typical FTIR spectrum without applying an electric field is shown in Figure 4a. The spectral peaks observed can be attributed to the IR-active molecular normal modes associated with either the cores or the alkyl chains of FLC molecules.[21] In Figure 4b, the infrared polarization-angle-dependent FTIR spectra were shown. The angular dependencies of the peaks associated with the FLC cores were found to be opposite of the stretching modes of the carboxylic group and CH_2/CH_3 of alkyl chains, indicating that the in-plane orientation-averaged IR-active molecular dipoles of the cores and alkyl chains are mutually perpendicular.[13] The peaks of the IR azimuthal patterns of the core groups deviate from the rubbing direction at $\Phi = 0°$, agreeing with the result of azimuthal pattern measurement of optical transmittance shown in Figure 3c.

We further analyzed the polarized IR spectra with the 2D-IR correlation technique,[21] and the results were presented in Figure 5. The field-free 2D synchronous plots $\Psi_s(\nu_1, \nu_2)$ in the 2820−

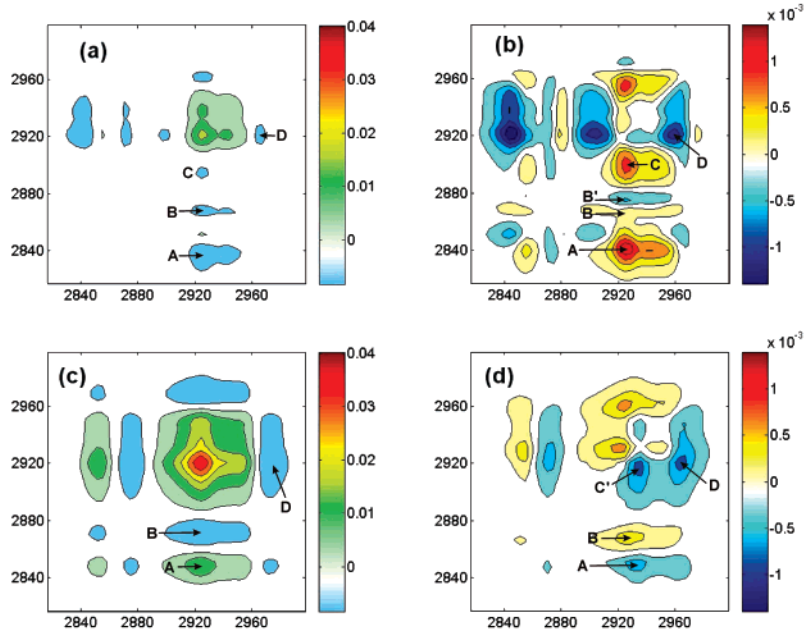

Figure 5. Synchronous $\Psi_s(\nu_1, \nu_2)$ (a and c: left column) and asynchronous $\Psi_a(\nu_1, \nu_2)$ (b and d: right column) 2D IR correlation plots from the alkyl-chain modes of SSFLC cells without (a and b: top row) and with *nc*-ZnO doping (c and d: bottom row).

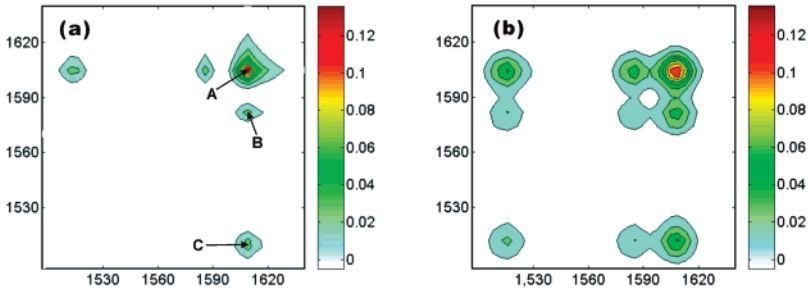

Figure 6. Synchronous $\Psi_s(\nu_1, \nu_2)$ 2D IR correlation plots from the core groups of SSFLC cells (a) without and (b) with *nc*-ZnO doping.

3000 cm^{-1} region were shown on the left column and the asynchronous $\Psi_a(\nu_1, \nu_2)$ on the right-hand side for the undoped (first row) and the *nc*-ZnO doped (second row) SSFLC cells.

The major auto-peak of $\Psi_s(\nu_1, \nu_2)$ appears at 2926 cm^{-1}, which can be assigned to the antisymmetric stretching of the CH_2 group (*a*-CH_2), reflects an in-plane alignment order of *a*-CH_2. The appearance of the cross-peaks A: 2926 (*a*-CH_2) versus 2840 cm^{-1} (*s*-CH_2), B: 2926 versus 2876 cm^{-1} (*s*-CH_3), C: 2926 (*a*-CH_2) versus 2900 cm^{-1} and D: 2975 (*a*-CH_3) versus 2926 cm^{-1} indicates the IR-active dipoles of CH_2 and CH_3 to be angularly correlated. Notice that the asynchronous cross-peak $\Psi_a(\nu_1, \nu_2)$ reflects relative orientation difference of IR-active dipoles. Therefore, two cross-peaks B and B′ in Figure 5b can be identified to be the *s*-CH_3 from different species. The cross-peaks A, B, and C were found to be positive while B′ and D were negative. By defining Φ_0 as the apparent angle of the maximum IR absorbance, the asynchronous cross-peak can be expressed as $\Psi_a(\nu_1, \nu_2) = 0.11 \sin 2[(\Phi_0(\nu_1) - \Phi_0(\nu_2)]$.[21] Therefore, the experimental finding shown here indicates that IR-active modes associated with the cross-peaks A, B, and C relative to that of the *a*-CH_2 mode at 2926 cm^{-1} have a smaller Φ_0 while peaks B′ and D have a larger Φ_0.

The major auto-peak of $\Psi_s(\nu_1, \nu_2)$ of the SSFLC doped with *nc*-ZnO appearing at 2926 cm^{-1} (*a*-CH_2) is more intense than the undoped sample, indicating an improved alignment order with *nc*-ZnO doping. In addition, for the doped sample the cross-peak features of C′ and D become in-phase, suggesting that CH_2 and CH_3 in the doped SSFLC are packed into a more ordered structure. This shall happen only when the ZnO nanodots are dispersed uniformly in the FLC medium. The TPM capping agent that favorably interacts with the FLC medium could be the key factor to achieve the uniform dispersion. Because ZnO nanocrystals are dispersed homogeneously and tie up the surrounding FLC dipolar species, we shall observe simplified CV characteristics with *nc*-ZnO doping as shown in Figure 3b.

In Figure 6, $\Psi_s(\nu_1, \nu_2)$ from the core groups of the FLC were presented. The cross-peaks of C(1514 vs 1608 cm^{-1}), B(1584 vs 1608 cm^{-1}) are more distinctive with *nc*-ZnO doping, indicating a more ordered structure of the core modes in the doped SSFLC cell.

The switching behavior of SSFLC can be better resolved by monitoring the field-induced reorientation of molecular fragments with the time-resolved 2D IR correlation technique. Although the asynchronous 2D correlation can be used to reflect the orientational variation, it is affected by the IR absorption peak height too. Therefore, instead we used a global 2D phase to show the orientational variations of IR-active modes. The time-resolved global phase can be calculated by using $\tan^{-1}[\Psi_a(\nu_1, t; \nu_1, 0)/\Psi_s(\nu_1, t; \nu_1, 0)]$.[20] The resulting phase angles of 2D IR correlation of the IR-active modes associated with the FLC cores and alkyl chains are presented in Figure 7a. It was found that the phase angles change sign with the polarity of the driving field, indicating that during the field-induced reorientation the IR-active molecular dipoles projected onto the substrate surface point to two opposite sides of their corresponding field-free directions.[21] Notice that even the core segments may belong to

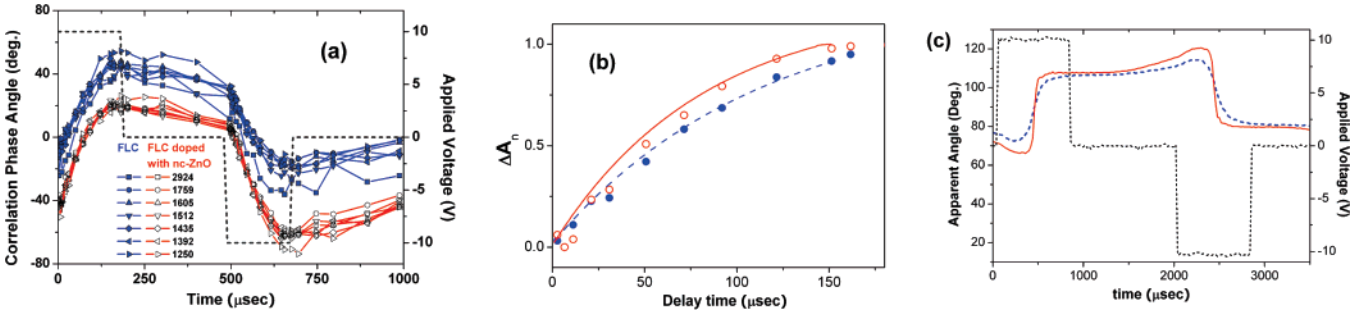

Figure 7. Time courses of 2D IR correlation phase angles of IR-active molecular normal modes of SSFLC with (open symbols) or without (filled symbols) *nc*-ZnO doping. The dashed line denotes the wave form of applied electric field. (b) The expanded view of the dynamic rising curves at 1759 cm^{-1}. (c) The corresponding variation curves of the electro-optical response of SSFLC with (solid curve) or without (dashed curve) *nc*-ZnO doping driven by a bipolar square wave at 250 Hz.

different species; they are tied up together. Those CH_2/CH_3 stretching modes associated with the alkyl chains are loosely connected, resulting in the observed larger angular spread than that the core groups. The orientational variations of the IR-active dipoles of the *nc*-ZnO doped SSFLC exhibit smaller angular spread than that of the undoped sample, suggesting doping with *nc*-ZnO to have more concerted reorientation processes.

The response times of molecular segments can be estimated from the rising edges of the switching curves, which are more distinguishable in the expanded view of the normalized phase angle variations of shown in Figure 7b. In the Figure, we specifically compare the C═O group at 1763 cm^{-1}, which makes a major contribution to the spontaneous polarization of SSFLC. For the undoped SSFLC cell (filled circles), the rising time of the C═O group was found to be 111 μs, slightly shorter than 128 μs of the C═C mode (not shown). For the *nc*-ZnO doped SSFLC cell (open circles), the C═O group was found to react faster to the applied field with a rising time of 82 μs. The response time of the C═C stretching mode of the *nc*-ZnO doped SSFLC cell remains essentially unchanging. The variation curves of the electro-optical response of SSFLC with (solid curve) or without (dashed curve) *nc*-ZnO doping driven by a bipolar square wave at 250 Hz are presented in Figure 7c for reference.

Discussion

For SSFLC, the angular equation of motion of FLC director can be described by

$$\gamma_c \frac{d\phi(t)}{dt} = -P_s E \cos \phi(t) \qquad (4)$$

Equation 4 yields a solution of $\tan[\phi(t)/2] = -1 + 2(1 - e^{-t/t_R})$ with $t_R = \gamma_c/P_s E$. By using the following data of FELIX 017/100: $\gamma_c = 8 \times 10^{-6}$ N s cm^{-2}, $P_s = 10.5$ nC cm^{-2}, and an applied field strength $E = 6.7 \times 10^4$ V cm^{-1}, we estimated $t_R = 114$ μs, which agrees well with the observed response times of C═C stretching mode and the electro-optical signal shown in Figure 7.

The field-induced reorientation can be modeled properly with a generalized variable $\Omega_i(t)$ that characterizes the extent to which the FLC molecule is out of its equilibrium conformation during switching. By using $\Omega_i(t)$ to represent the mean generalized angle between a specific functional group *i* and the axis of FLC core, this effective mechanical model determines a time dependence of $\Omega_i(t)$ for the viscous response of liquid crystals.[31] For a molecular fragment, which is directly coupled to the FLC director with a coupling coefficient ξ_i, the angular equation of motion of the fragment becomes

$$\gamma_c \frac{d[\Omega_i(t) - \xi_i \phi(t)]}{dt} = -P_s E \cos \phi(t) \qquad (5)$$

For fast switching of the fragment the solution for the generalized angle becomes $\Omega_i(t) = \xi_i \phi(t)$. We can estimate the effective response of the fragment with $1/t_R' = d\Omega_i(t)/dt|_{t=0} = \xi_i/t_R$. The observed faster response of the C═O group in the *nc*-ZnO doped SSFLC to an applied field can therefore be ascribed to originate from an increased coupling strength $\xi_i = 1.4$.

We proposed the improved alignment in both steady-state and dynamics with *nc*-ZnO doping to originate from a dipole−dipole interaction between the *nc*-ZnO and C═O groups of the surrounding FLC molecules. Dielectric dispersion measurements on spherical CdSe nanocrystallites suggest these quantum dots to have an internal electrostatic polarization resulting from a dipole moment that scales with the nanocrystal size.[32] The dipole moment was found to be only mildly screened by passivation layer. Similar to CdSe quantum dots, ZnO possesses a wurtzite structure that allows the ZnO nanoparticles of $2R_0 = 3.2$ nm to carry a dipole moment of $\mu_{ZnO} = 50$ D.[32] In the SSFLC, the particles being nanosize objects behave like a molecular dopant. At a uniform doping level of 1 wt %, we estimated that there are $n_{FLC} = 15\,000$ FLC molecules surrounding one ZnO nanoparticle in a spherical space of $R_{max} = 14$ nm. Each ZnO nanodot can exert a dipolar interaction with surrounding FLC molecules. The thermally averaged dipole−dipole interactive energy density can be calculated with

$$U_a^{ZnO-LC} = -\frac{2\mu_{CO}^2 \mu_{ZnO}^2 n_{FLC} N_{ZnO}}{3(4\pi\epsilon_0)^2 k_B T R_0^3 R_{max}^3}$$

We estimated $U_a^{ZnO-FLC} = -1000$ J·m^{-3} with $N_{ZnO} = 1.4 \times 10^{23}$ m^{-3}, $\mu_{CO} = 1.5$ D, $\mu_{ZnO} = 50$ D, and $k_B T = 4 \times 10^{-21}$ J. The stability gained by the *nc*-ZnO doping has an effect similar to that within 100-nm distance to an alignment surface with a fairly strong anchoring strength of 1×10^{-4} J·m^{-2}. This calculated energy density, however, is still too small to cause a detectable shift of transition temperature,[33] which agrees with our experimental observation.

Conclusions

We had discovered that by doping FLC with ZnO nanocrystals we can form an improved alignment structure compared to

that in an undoped SSFLC cell. Our 2D IR correlation data revealed that the ZnO nanocrystals were dispersed uniformly into the SSFLC medium used. This uniform dispersion yields stronger correlations among the IR-active modes from a dipole interaction of the ZnO nanodot with surrounding C═O groups of FLC molecules. The stronger correlations also lead to a more concerted reorientation dynamics. A molecular binding effect originating from a dipole interaction of a ZnO nanodot with surrounding C═O groups of FLC molecules was proposed to deduce a doping-induced binding effect with an energy stability of about 1000 J/m^3. The doping-induced binding effect might be useful to stabilize the layer structure without sacrificing the fast response of FLC materials. The method opens up an effective way to tailor FLC materials by blending instead of synthesizing new mesogenic molecules.

Acknowledgment. We acknowledge the financial support from the National Science Council of the Republic of China under grant NSC 95-2112-M-009-031-MY2.

References and Notes

(1) Clark, N. A.; Lagerwall, S. T. *Appl. Phys. Lett*. **1980**, *36*, 899.
(2) Lagerwall, S. T. *Ferroelectric and Antiferroelectric Liquid Crystals*; Wiley−VCH: Weinheim, 1999.
(3) Marinelli, M.; Ghosh, A. K.; Mercuri, F. *Phys. Rev. E* **2001**, *63*, 061713.
(4) Shiraishi, Y.; Toshima, N.; Maeda, K.; Yoshikawa, H.; Xu, J.; Kobayashi, S. *Appl. Phys. Lett*. **2001**, *81*, 2845.
(5) Kaur, S. S.; Singh, S. P.; Biradar, A. M.; Choudhary, A.; Sreenivas, K. *Appl. Phys. Lett*. **2007**, *91*, 023120.
(6) Park, J. H.; Lee, W. J.; Kim, J. H.; Lee, S. D. *Jpn. J. Appl. Phys*. **2003**, *42*, *Part 2*, L1155.
(7) Sigarev, A. A.; Vji, J. K.; Lewis, R. A.; Hird, M.; Goodby, J. W. *Phys. Rev. E* **2003**, *68*, 031707.
(8) Hide, F.; Clark, N. A.; Nito, K.; Yasuda, A.; Walba, D. M. *Phys. Rev. Lett*. **1995**, *75*, 2344.
(9) Verma, A. L.; Zhao, B.; Jiang, S. M.; Sheng, J. C.; Ozaki, Y. *Phys. Rev. E* **1997**, *56*, 3053.
(10) Shilov, S. V.; Skupin, H.; Kremer, F.; Wittig, T.; Zentel, R. *Phys. Rev. Lett*. **1997**, *79*, 1686.
(11) Verma, A. L.; Zhao, B.; Terauchi, H.; Ozaki, Y. *Phys. Rev. E* **1999**, *59*, 1868.
(12) Kocot, A.; Wrzalik, R.; Orgasinska, B.; Perova, T.; Vij, J. K.; Nguyen, H. T. *Phys. Rev. E* **1999**, *59*, 551.
(13) Verma, A. L.; Zhao, B.; Bhattacharjee, A.; Ozaki, Y. *Phys. Rev. E* **2001**, *63*, 051704.
(14) Noda, I. *Appl. Spectrosc*. **1993**, *47*, 1329.
(15) Shilov, S. V.; Skupin, H.; Kremer, F.; Wittig, T.; Zentel, R. *Macromol. Symp*. **1997**, *119*, 261.
(16) Nagasaki, Y.; Yoshihara, T.; Ozaki, Y. *J. Phys. Chem. B* **2000**, *104*, 2846.
(17) Nagasaki, Y.; Ozaki, Y. *Phys. Chem. Chem. Phys*. **2000**, *2*, 3037.
(18) Zhao, J. G.; Yoshihara, T.; Siesler, H. W.; Ozaki, Y. *Phys. Rev. E* **2001**, *64*, 031704.
(19) Zhao, J. G.; Tatani, K.; Yoshihara, T.; Ozaki, Y. *J. Phys. Chem. B* **2003**, *107*, 4227.
(20) Ozaki, Y.; Noda, I. *Two-Dimensional Correlation Spectroscopy*; AIP: Melville, NY, 2000; Vol. 508.
(21) Huang, J. Y.; Shih, W. T. *J. Phys. C* **2006**, *18*, 7593.
(22) Goyal, D. J.; Agashe, C.; Takwale, M. G.; Bhide, V. G.; Mahamuni, S.; Kulkarni, S. K. *J. Mater. Res*. **1993**, *8*, 1052.
(23) Meulenkamp, E. A. *J. Phys. Chem. B* **1998**, *102*, 5566.
(24) Felix 017/100 FLC mixture, commercial room-temperature FLC mixture by Clariant (Frankfurt, Germany).
(25) Miller, S. L.; Schwank, J. R.; Nasby, R. D.; Rodgers, M. S. *J. Appl. Phys*. **1991**, *70*, 2849.
(26) Rahman, M.; Kundu, S. K.; Chaudhuri, B. K. *J. Appl. Phys*. **2005**, *98*, 024114.
(27) Yang, P.; Carroll, D. L.; Ballato, J.; Schwartz, R. W. *Appl. Phys. Lett*. **2002**, *81*, 4583.
(28) Shih, W. T.; Huang, J. Y.; Zhang, J. Y. *Liq. Cryst*. **2004**, *31*, 377.
(29) Noda, I. *Appl. Spectrosc*. **1993**, *47*, 1329.
(30) Morita, S. *2Dshige*; Kwansei-Gakuin University, 2004; http://sci-tech.ksc.kwansei.ac.jp/~ozaki/.
(31) Jang, W. G.; Clark, N. A. *Phys. Rev. E* **2001**, *63*, 031707.
(32) Shim, M.; Guyot-Sionnest, P. *J. Chem. Phys*. **1999**, *111*, 6955.
(33) Li, F.; Buchnev, O.; Cheon, C. I.; Glushchenko, A.; Reshetnyak, V.; Reznikov, Y.; Sluckin, T. J.; West, J. L. *Phys. Rev. Lett*. **2006**, *97*, 147801.